Nanoscale

RSC Publishing

PAPER

View Article Online
View Journal | View Issue

Direct growth of nanotubes and graphene nanoflowers on electrochemical platinum electrodes†

Cite this: *Nanoscale*, 2013, **5**, 12448

Irene Taurino,*[a] Arnaud Magrez,[b] Federico Matteini,[c] László Forró,[d] Giovanni De Micheli[a] and Sandro Carrara[a]

Received 26th June 2013
Accepted 3rd October 2013

DOI: 10.1039/c3nr03283c

www.rsc.org/nanoscale

Multi-walled carbon nanotubes and graphene nanoflowers were grown by a catalytic chemical vapor deposition process on metal surfaces. Electrodeposition was used as a versatile technique to obtain three different iron catalyst coatings on platinum microelectrodes. The influence of growth parameters on carbon deposits was investigated. Characterization was carried out by scanning electron microscopy and Raman spectroscopy. A chemical treatment in sulphuric acid produced an increased voltammetric background current. In Raman spectra, the effect of the chemical treatment is seen as a more pronounced sp^3 hybridisation mode of C resulting from surface functionalization of the C nanomaterials. Overall, the hybrid electrodes we produced exhibit a promising performance for oxidase-based array biosensors. Therefore, our study opens the possibility of integrating the hybrid electrodes in biochip applications.

1. Introduction

Electrochemical sensors are powerful tools for the detection of certain compounds. Their fabrication methods are inexpensive and perfectly reproducible, and they can be used for simple analytical measurements with excellent sensitivity.[1] In addition, electrodes can easily be miniaturized to improve the time response, increase the signal-to-noise ratio and reduce the influence of the solution resistance.[2] Monitoring endogenous metabolites such as glucose and lactate in human fluids is of significant importance for diagnostic and therapeutic purposes.[3] The electrochemical determination of these molecules – always mediated by an enzyme – is indirectly achieved by detecting hydrogen peroxide, a product of the enzymatic reaction.[4]

Electrodes made of common metals or alloys are not sensitive enough to detect biomolecules of medical interest at their lowest physio-pathological concentrations. Therefore, many nanomaterials are currently employed to enhance biodetection.[5] Because of their attractive electrochemical properties, carbon materials, especially multi-walled carbon nanotubes (MWCNTs)[6] and graphene,[7] are of particular interest for nanostructuring electrodes. Several procedures have been developed to integrate graphene and CNTs onto electrodes. In most cases, additives or polymers are also incorporated together with these carbon nanomaterials.[8,9] Unfortunately, the presence of binders negatively affects the detection performance of the device by partially offsetting the electrical properties of the nanostructures, while preventing, at the same time, a high electric coupling between the nanomaterials and the metal substrates. Growth of graphene and CNTs onto electrodes by direct chemical vapor deposition (CVD) would ensure a close nanostructure–metal electric contact that is of crucial importance for high performance characteristics.

Graphene is commonly produced on a metal foil (generally Ni or Cu).[10] Conversely, growing MWCNTs on metals is difficult because catalytic particles are more active when supported by oxides. When placed on metal surfaces, catalytic particles are often poisoned because of the alloying.[11]

Here, we demonstrate the possibility of growing MWCNTs and flower-shaped nanographene onto Pt microelectrodes. First, for a selective deposition of the catalyst onto Pt, we developed versatile methods based on electrodeposition rather than on long and expensive procedures like metal evaporation and sputtering. Electrodeposition allows to efficiently deposit the catalyst in the form of nanoparticles as well as layers with controlled thickness. Another key advantage is the compatibility of this deposition method with electrochemical devices. We exploited the versatility of this procedure to obtain different iron deposits onto Pt electrodes. Second, we showed that the type of carbon nanostructures grown on Pt electrodes varies

[a]*Laboratory of Integrated Systems, EPFL – École Polytechnique Fédérale de Lausanne, Lausanne, Switzerland. E-mail: irene.taurino@epfl.ch; Fax: +41 21 69 34 225; Tel: +41 21 69 36878*

[b]*Crystal Growth Facility, EPFL – École Polytechnique Fédérale de Lausanne, Lausanne, Switzerland*

[c]*Laboratory of Semiconductor Materials, EPFL – École Polytechnique Fédérale de Lausanne, Lausanne, Switzerland*

[d]*Laboratory of Physics of Complex Matter, EPFL – École Polytechnique Fédérale de Lausanne, Lausanne, Switzerland*

† Electronic supplementary information (ESI) available. See DOI: 10.1039/c3nr03283c

with the nature of the catalyst. The influence of the deposition parameters on the characteristics of the obtained carbon materials was also examined. Their characterization was performed by SEM microscopy and micro-Raman spectroscopy. Third, the effectiveness of the nanostructured-electrodes after chemical activation was proven by recording voltammograms in hydrogen peroxide solutions.

2. Experimental setup

2.1. Microfabrication

We used a positive photoresist (AZ1512 on LOR) on Si wafers coated with a 500 nm SiO_2 layer. Platinum (200 nm) was deposited by evaporation (Alcatel EVA 600). A buffer layer of Ti (20 nm) was intercalated to improve the adhesion between Pt and SiO_2. After a lift-off process, platforms with electrodes having a diameter of 564 μm are obtained.

2.2. Iron electrodeposition

Linear scan voltammetry (LSV) and chronoamperometry (CA) were used to deposit an iron catalyst, in the form of a freshly prepared 0.2 M $FeSO_4$ solution (iron(II) sulfate heptahydrate *BioChemica*, AppliChem), onto the working electrodes. A buffer solution composed of 0.5 M H_3BO_3 (boric acid *BioChemica*, AppliChem) and 0.5 M NaCl (sodium chloride, *Sigma*) was used. All solutions were prepared with Milli Q (Millipore) water.

Three kinds of electrodeposited iron were tested as catalysts. Depositions were obtained by (i) LSV with a potential window of 0/−1.4 V and a scan rate of 5 mV s^{-1}, followed by solution stirring for approximately three minutes (LSV + STIR), (ii) CA at −1.4 V for 15 s followed by solution stirring for approximately three minutes (CA15 + STIR), (iii) CA at −1.4 V or −1.3 V for 60 s (CA60). All the experiments were performed under aerobic conditions. A gold circular electrode (diameter = 4 mm), placed in parallel and approximately at 1 cm from the working electrode, was used as a counter electrode to obtain homogeneous depositions.

2.3. Synthesis of carbon nanomaterials

MWCNTs and graphene-shaped deposits were grown onto the different iron coatings in a CCVD quartz tube furnace at ambient pressure. Prior to growth, the devices were introduced in the furnace (pre-heated at growth temperature) and kept there for 10 minutes under a H_2 and Ar flow (60 l h^{-1}). This resulted in catalyst film dewetting and particle formation. C materials were deposited by oxidative dehydrogenation chemistry;[12,13] Ar was introduced in the CVD reactor at 45 l h^{-1} together with C_2H_2 and CO_2 (with a 1 : 1 ratio and a flow rate of 0.25 l h^{-1}) for 5 minutes. The growth temperature was fixed at 750 °C. After the deposition, the chamber was cleaned under an Ar flow (60 l h^{-1}) for 10 minutes. To sum up, standard growths were obtained with the following parameters (standard parameters): 10 minutes of annealing, 5 minutes of deposition, a C_2H_2 gas flow of 0.25 l h^{-1}, a CO_2 gas flow of 0.25 l h^{-1} and a growth temperature of 750 °C.

2.4. Materials characterization

The surface morphology and the roughness of the Fe catalyst before and after segregation were examined with a Bruker Atomic Force Microscope. The roughness parameters of the surface were evaluated with a Gwyddion software[14] after plane subtraction and horizontal scar removal. A Zeiss MERLIN Scanning Electron Microscope was used to investigate the morphology of both the catalyst and carbon materials. We measured the covered area of the catalyst nanoparticles and the average CNT diameters by using ImageJ software.[15] Raman spectra were acquired using a homemade micro-Raman microscope.[16] The spectra were analysed with a triple grating spectrometer (TriVista 555). A 488 nm laser was focused on a diffraction-limited spot of around 0.65 μm^2 to reach a power density of 2.2–2.3 mW μm^{-2}. The acquisition time varied from 2 to 5 minutes. Particular care was taken to avoid heating of the samples because of the well-known possibility of modifying/damaging the C nanomaterials with the laser.[17] Igor Pro (Wavemetrics, Lake Oswego, OR, USA) software was employed to fit Raman peaks using Lorentzians.[18]

2.5. Activation and electrochemistry

The as-grown carbon nanomaterials were activated in 6 M H_2SO_4 (Sigma, 95–98% vol) for 6 hours. A 0.01 M Phosphate Buffer Saline (PBS, pH 7.4, Sigma) and 1 mM H_2O_2 (30% vol) solution was used for electrochemical measurements.[19] Measurements were carried out with a three electrode configuration electrochemical cell. The microfabricated Pt electrodes were employed as working electrodes. The counter and reference electrodes were made of Pt and Ag/AgCl (3 M KCl), respectively. Cyclic voltammograms (CVs) were registered with a Versastat 3 potentiostat (Princeton Applied Technologies) and VersaStudio software. Initially, electrode potentials were cycled between two potential limits until two perfectly overlapping subsequent voltammograms were obtained.[20]

3. Results and discussion

3.1. Production and characterization of the iron catalyst

Fig. 1(a) and (d) show SEM images of iron nanoparticles (FeNPs) obtained with the LSV + STIR procedure. The covered area is (27.6 ± 3.8)% and the perimeter of the particles is (245.7 ± 29.3) nm. The minimum and the maximum near-neighbour distances between nanoparticles were estimated to be (26.6 ± 5.6) nm and (164.8 ± 20.8) nm, respectively. From FeNPs exhibiting such characteristics, Pt microelectrodes fully covered with MWCNTs were obtained (for further details see the ESI†). Using the CA15 + STIR deposition, platinum electrodes were covered with a non-compact iron layer (FeNC). Arrows in Fig. 1(b) and (e) highlight the presence of cracks on the Fe coating. Platinum is clearly visible under the FeNC layer. Conversely, compact iron layers (FeC) do not show any fissure and the coating is thicker than FeNC. This is due to the four-fold increase in the electrodeposition time (Fig. 1(c) and (f)).

Following the iron electrodeposition, coatings were annealed at growth temperature under an Ar and H_2 flow. Fig. 2(a–c) show

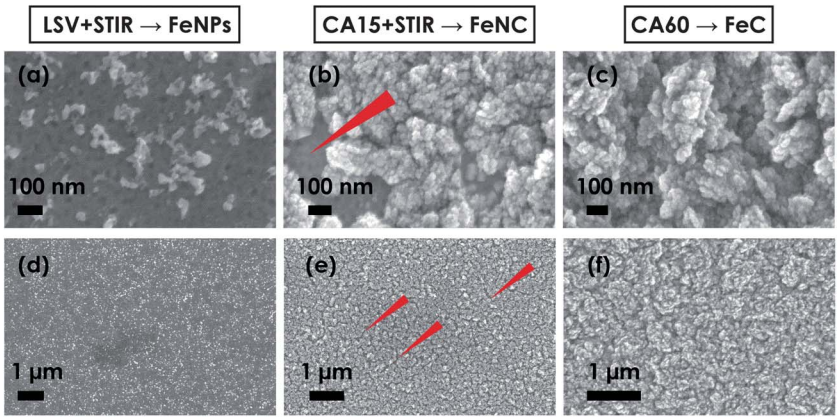

Fig. 1 SEM images at high (a–c) and low (d–f) magnification of iron electrodeposited onto Pt microelectrodes by using the procedure (a–d) LSV + STIR (b–e) CA15 + STIR and (c–f) CA60.

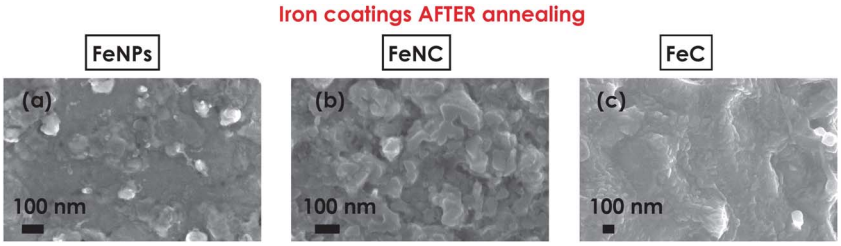

Fig. 2 SEM images of iron electrodeposited onto Pt electrodes and obtained with (a) LSV + STIR (b) CA15 + STIR and (c) CA60 after 10 minutes of annealing at 750 °C.

SEM images of the different iron layers after 10 minutes of annealing at 750 °C. The roughness, evaluated by AFM (Fig. 3), does not differ significantly between FeNPs and FeNC (R_{rms} was 34.8 nm and 29.6 nm for FeNPs, and 22.7 nm and 25.0 nm for FeNC, before and after annealing, respectively). This behaviour is different in the case of FeC for which R_{rms} decreases remarkably after the annealing (from 54.1 nm to 38.6 nm). Particles are still present in FeNPs and FeNC. Undulated surfaces with clear stripes result from FeC.

3.2. Effects of synthesis parameters

Carbon materials were imaged by SEM. From FeNPs, sparse rolls of MWCNTs were selectively grown onto the metal electrodes (Fig. 4(a)). Randomly oriented nanotubes resulted from FeNC (Fig. 4(b)). Average diameters of the MWCNTs grown from FeNPs and FeNC were (15.4 ± 4.0) nm and (13.7 ± 3.2) nm, respectively. Fig. 4(c) shows nanographene-shaped petals resulting from FeC. A top view of a uniform nanostructured electrode with nanographene-shaped flowers is shown in Fig. 5.

We investigated the effect of different deposition variables on the resulting carbon materials. The same kind of nanographene-shaped material was observed when the growth parameters were changed (temperature, flow of the carbon gas, annealing time). We also obtained nanographene from compact layers of electrodeposited Co and Fe_2Co, which are effective catalysts for the deposition of ordered C nanomaterials.[21] An increase in the yield resulted from a prolonged carbon growth time and greater catalyst thickness.

We examined the influence of growth temperature on the average MWCNT diameter. In general, the MWCNT diameter increased by reducing the growth temperature. The formation of thick and short CNTs was observed at 600 °C (Fig. 6). When FeNC was used as the catalyst, the CNT diameter increased more as the temperature decreased. Moreover, lowering the temperature means that less iron is catalytically active for nanotube nucleation and so the growth kinetics is reduced. This phenomenon results in a smaller CNT yield.

We reduced the catalyst annealing time from 10 to 3 minutes. From FeNPs we obtained MWCNTs with a slightly wider diameter (16.9 ± 3.2 nm). From FeNC, the increase in diameter was more pronounced (19.5 ± 5.3 nm – Fig. 7(b)). The dewetting of the Fe film by thermal annealing has been extensively reported in the literature.[22] In some studies the procedure was very similar to the one we followed.[23] A shorter annealing time limits the Fe film dewetting, resulting in bigger Fe nanoparticles and, thus, in larger MWCNTs. To prove this assumption, we measured the FeNP size after two different annealing times. The average diameter of the FeNPs was 14.5 ± 5.3 nm and 16.0 ± 4.7 nm after 10 and 3 minutes of annealing, respectively. As expected, the increase of the particle size was more evident from FeNC (14.2 ± 3.9 nm after 10 minutes and 21.7 ± 8.9 nm after 3 minutes of annealing).

With a growth temperature of 750 °C and an annealing time of 10 minutes, an increase in the carbon precursor flow (from

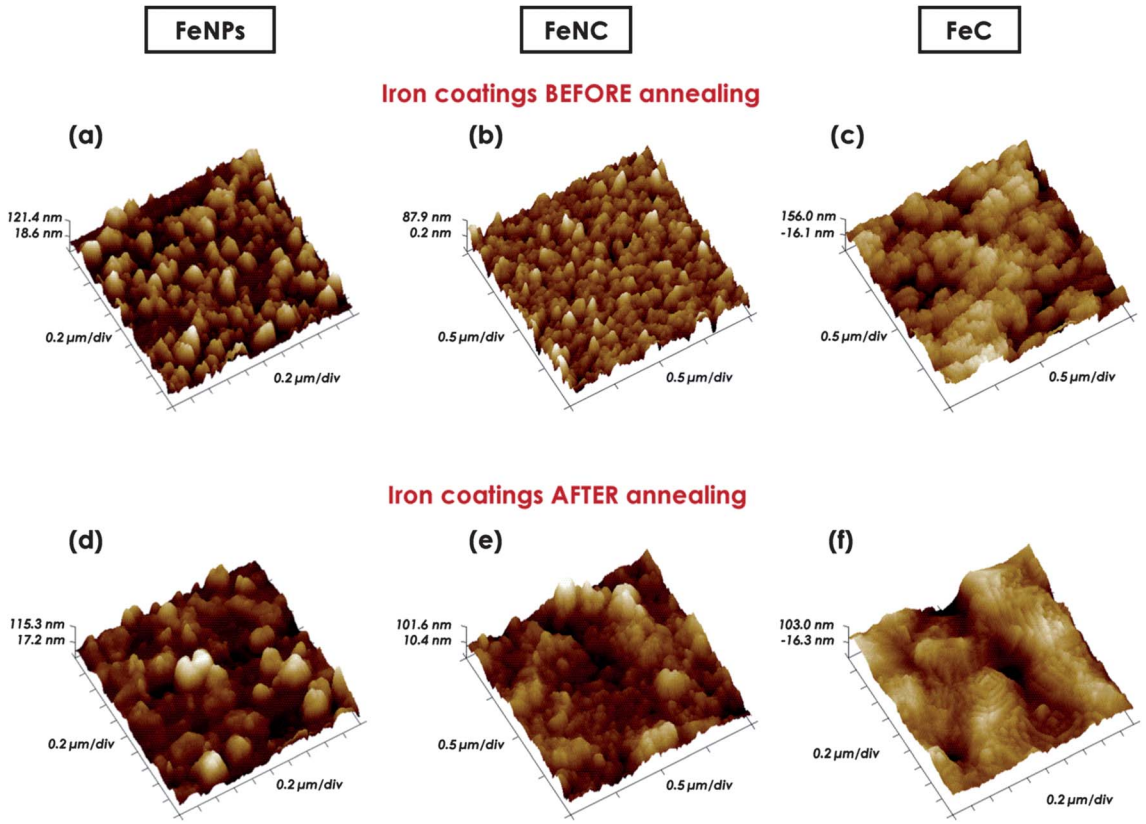

Fig. 3 3D AFM images (Nanoscope Analysis software) before (a–c) and after (d–f) 10 minutes of annealing at 750 °C (procedures: LSV + STIR (a–d) CA15 + STIR (b–e) and CA60 (c–f); images: 2 µm × 2 µm).

0.25 l h^{-1} to 0.5 l h^{-1} for both C_2H_2 and CO_2) does not vary the diameter of CNTs (11.5 ± 2.1 nm) grown from FeNPs. Conversely, the doubling of the carbon flux promotes the formation of nanotubes with a broader range of diameters (from 10 to 70 nm) from FeNC. This is due to the catalytic activation of larger Fe nanoparticles if the furnace is fed with a higher carbon flux, which in turn gives rise to nanotubes with larger diameters (Fig. 7(c)).

We also studied the effect of tripling the carbon growth time (from 5 to 15 minutes). Also in this case, we noted an almost unvaried average diameter of the tubes grown from FeNPs (15.8 ± 4.2 nm). In contrast, the diameter of the tubes obtained from FeNC doubled (34.9 ± 6.4 nm – Fig. 7(d)). It is reasonable to assume that, in the presence of the available catalyst, a prolonged carbon feed results in MWCNTs with more graphitic layers.

One cannot exclude the presence of carbon nanofibers together with CNTs in some samples. This is especially true when the catalytically active particles are big in size (*e.g.*, lower synthesis temperature, shorter annealing period).

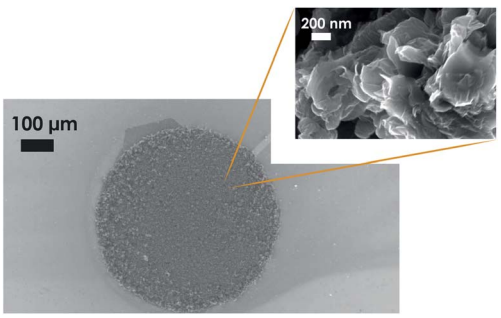

Fig. 5 Top view of a nanostructured Pt microelectrode with graphene-shaped flowers.

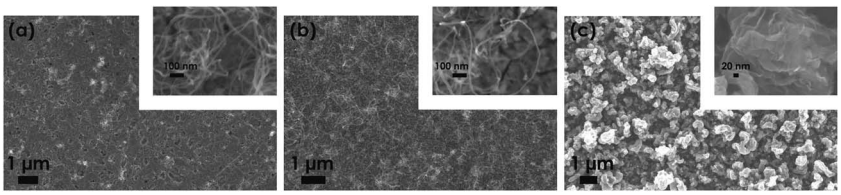

Fig. 4 SEM images of MWCNTs (a–b) and graphene-shaped nanostructures (c) at lower and higher magnification (insets) deposited on Pt and obtained from FeNPs (a), FeNC (b) and FeC (c), respectively (annealing time: 10 minutes, carbon growth time: 5 minutes, growth temperature: 750 °C).

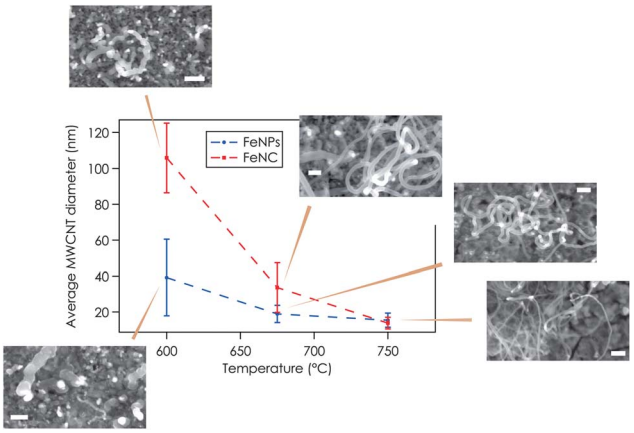

Fig. 6 Evolution of the MWCNT diameter with the temperature in the case of growths from FeNPs (blue line) and FeNC (red line). SEM images of MWCNTs were selected for each deposition condition (bars: 100 nm).

3.3. Characterization by micro-Raman spectroscopy

A selected number of samples was analyzed by micro-Raman spectroscopy. Each spectrum consists of three typical bands.[24,25] D is the defect- and disorder-induced band ($\approx$1350 cm^{-1}). The G band is a measure of the graphitic lattice quality ($\approx$1580 cm^{-1}) and the G′ band – overtone of the D peak, $\approx$2710 cm^{-1} – is also sensitive to the density of defects. The relative integrated peak ratios were considered for the structural evaluation of the materials[24] since less sensitive to the experimental conditions than the absolute intensities.[25]

The ratio does not show substantial changes among MWCNTs with diameters in the 10–20 nm range ($I_d/I_g \approx 1$). Conversely, we noted a strong increase of I_d/I_g for wider and shorter tubes ($\approx$1.7) grown at 600 °C, indicating a less perfect crystalline lattice.[18] The high defect density of these tubes was also confirmed by the simultaneous decrease of both $I_{g'}/I_g$ and $I_{g'}/I_d$ ratios.[25] The values of the full width at half maximum (FWHM) of all the three peaks were found to be approximately 20–30 cm^{-1} higher for CNTs grown at 600 °C than for MWCNTs fabricated at higher temperatures, indicating the presence of more disordered and amorphous carbon in the samples prepared at 600 °C.[26]

Nanographene-shaped structures showed the lowest value of I_d/I_g ($\approx$0.6) and the highest $I_{g'}/I_g$ and $I_{g'}/I_d$ ratios (approximately 3 and 5, respectively). The ratio $I_{g'}/I_g$ resulted to be 9 times higher than that measured from graphite. Also $I_{g'}/I_d$ showed a very high value (13 times higher than graphite). Narrow peaks characterize these carbon nanostructures. FWHM values were about 45 cm^{-1}, 35 cm^{-1} and 65 cm^{-1} for G, D and G′ peaks, respectively. We noticed that the G band does not present the characteristic shoulder of graphite-based materials (Fig. 8(a)). In addition, the position of the G′ peak was about 20 cm^{-1} lower than that related to graphite. This peak is also sharper and almost 4 times more intense than the G′ peak of graphite (Fig. 8(b)). Considering these data, we can argue to have obtained flowers of nanographene from FeC electrodeposited on Pt.[27] Generally Ni and Cu are used as catalysts to grow graphene.[10] The iron layer represents a valuable possibility to produce graphene flakes. In this case, the use of acetylene as the carbon source has been demonstrated to allow a drastic reduction of the growth temperature during the process. This is extremely promising for the direct integration of graphene onto devices with electronic circuits.[28] Up to now, only a few studies have focused on graphene deposited onto Fe[29] due to the difficulty of controlling carbon diffusion and precipitation, with consequent formation of mixed phases. Moreover, to the best of our knowledge, this is the first experimental study that reports the deposition of graphene flakes onto electrodeposited Fe. It is reasonable to assume that a very thin layer of iron remains between the graphene petals and the Pt.[30] The objective of the present work was to avoid the use of a dielectric underlayer (placed between Pt and iron) for growing carbon nanostructures, since it would have created a high contact resistance. Certainly, a direct coupling carbon nanostructure-metal is still present even if a thin layer of iron is interposed between the two materials.

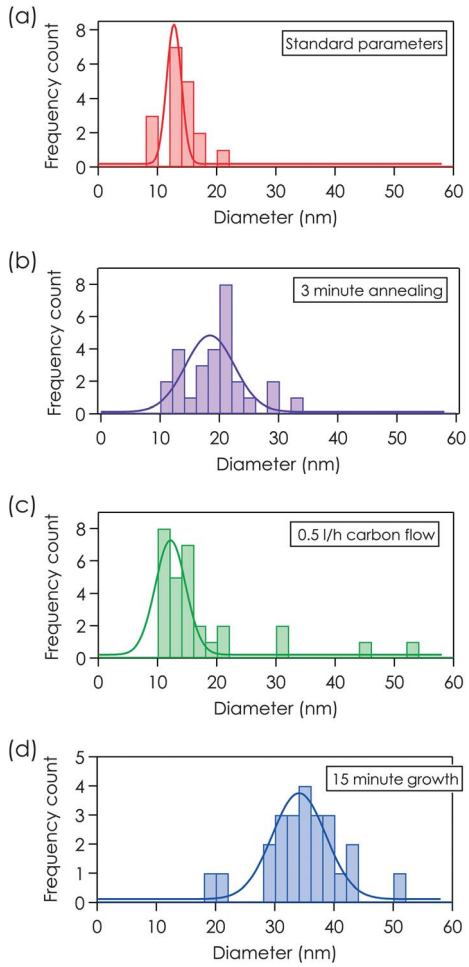

Fig. 7 Diameter distribution of MWCNTs produced from FeNC under different growth conditions (first deposition (a), reduced annealing time (b), doubled flow of the carbon gas (c), and tripled carbon growth time (d)).

3.4. Carbon activation

Before studying the electrochemistry of the nanostructured Pt electrodes, we performed material activation. Different surface

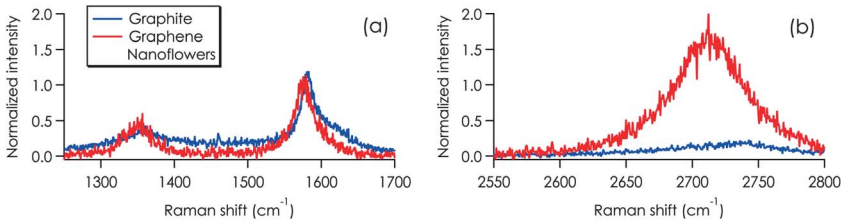

Fig. 8 Raman spectra of graphite (blue line) and nanographene flowers (red line) in the ranges (a) 1200–1700 cm^{-1} and (b) 2550–2800 cm^{-1}. All the spectra were normalized with respect to the G peak height.

modifications of carbon materials can be employed. Thermal annealing of carbon materials at 400 °C–500 °C is one of the procedures currently used to form oxides and defect sites and to remove the amorphous carbon. However, this method compromises the mechanical stability of the nanomaterials on the electrodes.[31] Electrochemical procedures are not suitable for our carbon materials. These methods do not have any effects on the tube and graphene walls, creating functional groups and defects onto the graphene sheet edges and tube caps.[32,33] The carbon nanoflowers and MWCNTs we produced (randomly oriented with respect to the Pt surface) extensively expose their walls. Therefore, a chemical activation was chosen. Carbon nanomaterials were pretreated in a sulphuric acid solution[19] and the activation time was optimized to avoid material detachment from the surface (6 hours). Since an increase in the number of defects is expected after the activation, treated nanostructures should lead to better electron transfer in electrochemistry.[34]

To confirm the efficacy of the activation, Raman spectra were taken before and after the treatment. The increase in the peak intensity in the frequency region beyond 2900 cm^{-1} is indicative of the O–H stretching of acid-produced carboxylic groups.[35] Table 1 shows the increase of the ratios between the G peak and the peaks related to the introduction of defects after the activation (G + D1 peak at ≈3000 cm^{-1} and 2D2 peak at ≈3200 cm^{-1}).

3.5. Electrochemical study

The introduction of redox active surface groups was also confirmed by CVs.[33] Indeed, an increase in the charge calculated from the area of the voltammograms was registered.[36,37] Microelectrodes with MWCNTs synthesized at 600 °C showed a total capacitance of 0.217 μF and 0.576 μF before and after the treatment, respectively. This phenomenon was especially evident when more carbon material covered the electrode. Indeed, the higher carbon deposit yield obtained at 600 °C showed an increase in total capacitance of more than one order of magnitude (0.257 μF before and 8.901 μF after the activation).

The CVs of the nanostructured electrodes were recorded with H_2O_2. H_2O_2 was selected as an electroactive compound extensively used to monitor various metabolites.[4] In Fig. 9(a) it is possible to notice a small increase in the capacitive background current in the presence of short and low density tubes, with respect to the bare electrode. The series of peaks related to the hydrogen adsorption/desorption are less evident but still present. The voltammogram also shows a set of four peaks related to the characteristic oxido-reduction of H_2O_2 at the Pt surface.[38] This indicates that CNTs are so sparse that the electrolyte is able to spread onto the Pt electrode. Conversely,

Table 1 Increase of $I_{(g+d)}/I_g$ and I_{2d2}/I_g ratios after the carbon activation

	Before activation		After activation	
	Nanographene	MWCNTs	Nanographene	MWCNTs
$I_{(g+d)}/I_g$	0.42	0.39	1.52	1.16
I_{2d2}/I_g	0.21	0.10	1.23	0.19

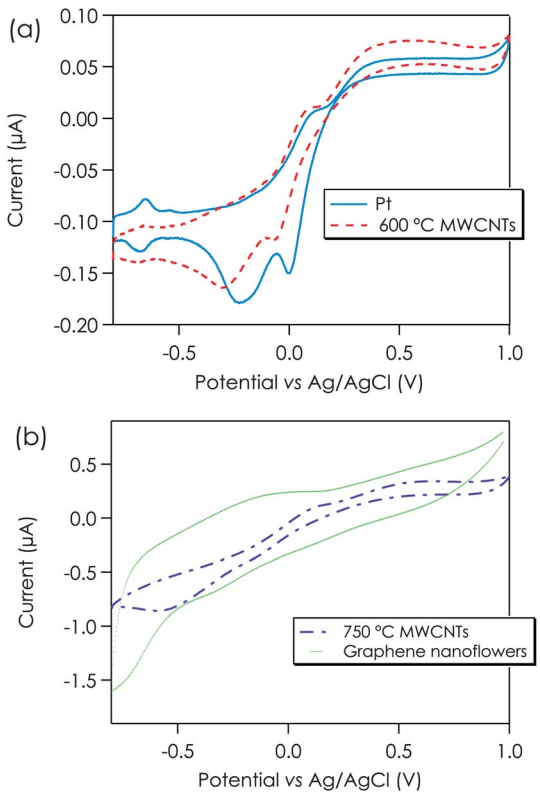

Fig. 9 (a) CVs of Pt (solid line in blue) and Pt nanostructured with MWCNTs grown at 600 °C (dotted line in red). (b) CVs of Pt nanostructured with MWCNTs (dash-dot line in violet) and Pt nanostructured with graphene nanoflowers (line in green) both grown at 750 °C. Solution: 1 mM of H_2O_2. Potential window: −0.8/+1 V. Scan rate: 0.05 V s^{-1}.

Table 2 Oxidation peak currents of H_2O_2 (1 mM) related to Pt electrodes and electrodes with three different kinds of integrated nanostructures

	Pt	600 °C MWCNTs	750 °C MWCNTs	Graphene Nanoflowers
Peak current (μA)	0.048	0.064	0.22	2.14

voltammograms of electrodes with incorporated MWCNTs and nanographene flakes produced at 750 °C do not present these features (Fig. 9(b)). The shapes of the related CVs are very close to those obtained with electrodes entirely composed of carbon-based materials.[39] Electrodes with MWCNTs produced at 750 °C and nanographene have a large capacitive current. Nanographene flowers also produce a peak characteristic of the activated carbon materials at approximately −200 mV.[40] Bare electrodes exhibited very poor electrochemical signals (no oxidation peak). Higher currents and better-defined oxidation peaks appear in voltammograms recorded with a higher CVD density of nanomaterials (Table 2). The peak current of nanographene structures shows an improvement of two and one orders of magnitude with respect to bare and CNT-nanostructured microelectrodes, respectively. In particular, if short MWCNTs improve only slightly the electrode performance (oxidation peak height higher than a bare electrode), MWCNTs and nanographene flowers deposited at higher temperatures yield the most intense peak currents. This is due to the greater amount of nanomaterials covering the electrodes.

4. Conclusion

We produced different carbon nanomaterials by CVD directly onto Pt microelectrodes. In the first stage, iron was deposited as the catalyst material. To this end, an electrodeposition technique was selected because it is an easy and rapid method for selective catalyst incorporation. Thanks to the versatility of this method, we obtained three different kinds of iron coatings. From iron nanoparticles and non-compact iron layers we obtained MWCNTs. Conversely, graphene-shaped structures were grown from compact iron coatings. Shorter, thicker and more defective nanotubes were obtained by lowering the deposition temperature. Other deposition variables only influence the diameter of nanotubes grown from a non-compact iron layer. Thicker tubes were produced by decreasing the annealing time and by increasing the flow of the carbon gas and the carbon growth time. Nanographene-shaped structures were grown from compact iron coatings regardless of the deposition conditions. We noticed a yield increase for an increased carbon growth time. A comparison between Raman spectra of this nanomaterial and graphite revealed that we had grown flowers of nanographene on Pt. This is the first experimental study that reports the production of graphene nanomaterials from electrodeposited Fe coatings.

All the deposited nanomaterials were acid activated to increase their electroactivity. The appearance of more pronounced defect modes in Raman spectra and the increase of the background current in CV confirmed the efficacy of the chemical treatment to produce electroactive and defective sites.[37] Voltammograms in solutions containing hydrogen peroxide revealed the suitability of these nanostructures for application in biosensing systems.

Acknowledgements

The authors thank Andrea Cavallini for the design of the microfabricated electrochemical electrodes, Anna Fontcuberta i Morral for the Raman set-up, Laurent Bernard for the preparation of the CVD system and Elena Della Vecchia for the revision of the manuscript. The research was supported by the i-IronIC project. The i-IronIC project was financed by a grant from the Swiss Nano-Tera.ch initiative and evaluated by the Swiss National Science Foundation. Arnaud Magrez acknowledges financial support from the SCOPES project no IZ74Z0_137458 and the European project NAMASEN. Federico Matteini acknowledges financial support from ERC grant UpCon.

References

1 W. Albery, P. Bartlett, A. Cass, D. Craston and B. Haggett, Electrochemical sensors: theory and experiment, *J. Chem. Soc., Faraday Trans. 1*, 1986, **82**(4), 1033–1050.
2 R. Forster, Microelectrodes: new dimensions in electrochemistry, *Chem. Soc. Rev.*, 1994, **23**(4), 289–297.
3 I. Moser, G. Jobst and G. Urban, Biosensor arrays for simultaneous measurement of glucose, lactate, glutamate, and glutamine, *Biosens. Bioelectron.*, 2002, **17**(4), 297–302.
4 J. Wang, *et al.*, Electrochemical glucose biosensors, *Chem. Rev.*, 2008, **108**(2), 814.
5 X. Luo, A. Morrin, A. Killard and M. Smyth, Application of nanoparticles in electrochemical sensors and biosensors, *Electroanalysis*, 2006, **18**(4), 319–326.
6 J. Gooding, Nanostructuring electrodes with carbon nanotubes: A review on electrochemistry and applications for sensing, *Electrochim. Acta*, 2005, **50**(15), 3049–3060.
7 Y. Shao, J. Wang, H. Wu, J. Liu, I. Aksay and Y. Lin, Graphene based electrochemical sensors and biosensors: a review, *Electroanalysis*, 2010, **22**(10), 1027–1036.
8 K. Zhang, L. Zhang, X. Zhao and J. Wu, Graphene/polyaniline nanofiber composites as supercapacitor electrodes, *Chem. Mater.*, 2010, **22**(4), 1392–1401.
9 K. Balasubramanian and M. Burghard, Biosensors based on carbon nanotubes, *Anal. Bioanal. Chem.*, 2006, **385**(3), 452–468.
10 C. Soldano, A. Mahmood and E. Dujardin, Production, properties and potential of graphene, *Carbon*, 2010, **48**(8), 2127–2150.
11 G. Nessim, D. Acquaviva, M. Seita, K. O'Brien and C. Thompson, The critical role of the underlayer material and thickness in growing vertically aligned carbon nanotubes and nanofibers on metallic substrates by chemical vapor deposition, *Adv. Funct. Mater.*, 2010, **20**(8), 1306–1312.

12 A. Magrez, J. Seo, R. Smajda, B. Korbely, J. Andresen, M. Mionć, S. Casimirius and L. Forró, Low-temperature, highly efficient growth of carbon nanotubes on functional materials by an oxidative dehydrogenation reaction, *ACS Nano*, 2010, **4**(7), 3702–3708.

13 A. Magrez, J. W. Seo, V. L. Kuznetsov and L. Forró, Evidence of an equimolar C_2H_2–CO_2 reaction in the synthesis of carbon nanotubes, *Angew. Chem.*, 2007, **119**(3), 445–448.

14 P. Klapetek, D. Nečas and C. Anderson, *Gwyddion user guide*, http://gwyddion.net/, 2004–2009.

15 W. Rasband, *ImageJ*, US National Institutes of Health, Bethesda, Maryland, USA, 1997.

16 B. Ketterer, M. Heiss, E. Uccelli, J. Arbiol and A. Fontcuberta i Morral, Untangling the Electronic Band Structure of Wurtzite GaAs Nanowires by Resonant Raman Spectroscopy, *ACS Nano*, 2011, **5**(9), 7585–7592.

17 D. Olevik, A. Soldatov, M. Dossot, B. Vigolo, B. Humbert and E. McRae, Stability of carbon nanotubes to laser irradiation probed by Raman spectroscopy, *Phys. Status Solidi B*, 2008, **245**(10), 2212–2215.

18 A. Sadezky, H. Muckenhuber, H. Grothe, R. Niessner and U. Pöschl, Raman microspectroscopy of soot and related carbonaceous materials: Spectral analysis and structural information, *Carbon*, 2005, **43**(8), 1731–1742.

19 Y. Chen, J. Huang and C. Chuang, Glucose biosensor based on multiwalled carbon nanotubes grown directly on Si, *Carbon*, 2009, **47**(13), 3106–3112.

20 L. Aldous, D. S. Silvester, W. R. Pitner, R. G. Compton, M. C. Lagunas and C. Hardacre, Voltammetric studies of gold, protons, and [HCl2]-in ionic liquids, *J. Phys. Chem. C*, 2007, **111**(24), 8496–8503.

21 A. Magrez, J. W. Seo, C. Mikó, K. Herndi and L. Forró, Growth of Carbon Nanotubes with Alkaline Earth Carbonate as Support, *J. Phys. Chem. B*, 2005, **109**(20), 10087–10091.

22 G. D. Nessim, A. J. Hart, J. S. Kim, D. Acquaviva, J. Oh, C. D. Morgan, M. Seita, J. S. Leib and C. V. Thompson, Tuning of vertically-aligned carbon nanotube diameter and areal density through catalyst pre-treatment, *Nano Lett.*, 2008, **8**(11), 3587–3593.

23 Y. Y. Wei, G. Eres, V. I. Merkulov and D. H. Lowndes, Effect of catalyst film thickness on carbon nanotube growth by selective area chemical vapor deposition, *Appl. Phys. Lett.*, 2001, **78**(10), 1394–1396.

24 S. Osswald, M. Havel and Y. Gogotsi, Monitoring oxidation of multiwalled carbon nanotubes by Raman spectroscopy, *J. Raman Spectrosc.*, 2007, **38**(6), 728–736.

25 R. DiLeo, B. Landi and R. Raffaelle, Purity assessment of multiwalled carbon nanotubes by Raman spectroscopy, *J. Appl. Phys.*, 2007, **101**(6), 064307.

26 A. Ferrari and J. Robertson, Interpretation of Raman spectra of disordered and amorphous carbon, *Phys. Rev. B: Condens. Matter Mater. Phys.*, 2000, **61**(20), 14095.

27 A. Ferrari, Raman spectroscopy of graphene and graphite: Disorder, electron–phonon coupling, doping and nonadiabatic effects, *Solid State Commun.*, 2007, **143**(1), 47–57.

28 D. Kondo, S. Sato, K. Yagi, N. Harada, M. Sato, M. Nihei and N. Yokoyama, Low-Temperature Synthesis of Graphene and Fabrication of Top-Gated Field Effect Transistors without Using Transfer Processes, *Appl. Phys. Express*, 2010, **3**(2), 025102.

29 N. A. Vinogradov, A. Zakharov, V. Kocevski, J. Rusz, K. Simonov, O. Eriksson, A. Mikkelsen, E. Lundgren, A. Vinogradov, N. Mårtensson, *et al.*, Formation and Structure of Graphene Waves on Fe (110), *Phys. Rev. Lett.*, 2012, **109**(2), 26101.

30 C. Miao, C. Zheng, O. Liang and Y.-H. Xie, Chemical vapor deposition of graphene, *Physics and applications of graphene-experiments*, 2011.

31 K. Wang, H. Fishman, H. Dai and J. Harris, Neural stimulation with a carbon nanotube microelectrode array, *Nano Lett.*, 2006, **6**(9), 2043–2048.

32 J. Ye, X. Liu, H. Cui, W. Zhang, F. Sheu and T. Lim, Electrochemical oxidation of multi-walled carbon nanotubes and its application to electrochemical double layer capacitors, *Electrochem. Commun.*, 2005, **7**(3), 249–255.

33 M. Musameh, N. S. Lawrence and J. Wang, Electrochemical activation of carbon nanotubes, *Electrochem. Commun.*, 2005, **7**(1), 14–18.

34 I. Taurino, S. Carrara, M. Giorcelli, A. Tagliaferro and G. D. Micheli, Comparing sensitivities of differently oriented multi-walled carbon nanotubes integrated on silicon wafer for electrochemical biosensors, *Sens. Actuators, B*, 2011, **160**(1), 327–333.

35 N. Chakrapani, S. Curran, B. Wei, P. Ajayan, A. Carrillo and R. Kane, Spectral fingerprinting of structural defects in plasma-treated carbon nanotubes, *J. Mater. Res.*, 2003, **18**(10), 2515–2521.

36 E. Kalu, T. Nwoga, V. Srinivasan and J. Weidner, Cyclic voltammetric studies of the effects of time and temperature on the capacitance of electrochemically deposited nickel hydroxide, *J. Power Sources*, 2001, **92**(1), 163–167.

37 J. Maruyama and I. Abe, Influence of anodic oxidation of glassy carbon surface on voltammetric behavior of Nafion-coated glassy carbon electrodes, *Electrochim. Acta*, 2001, **46**(22), 3381–3386.

38 I. Katsounaros, W. Schneider, J. Meier, U. Benedikt, P. Biedermann, A. Auer and K. Mayrhofer, Hydrogen peroxide electrochemistry on platinum: towards understanding the oxygen reduction reaction mechanism, *Phys. Chem. Chem. Phys.*, 2012, **14**, 7384–7391.

39 C. Domínguez, A. Quintanilla, P. Ocón, J. Casas and J. Rodriguez, The use of cyclic voltammetry to assess the activity of carbon materials for hydrogen peroxide decomposition, *Carbon*, 2013, **60**, 76–83.

40 S. Chatterjee and A. Chen, Functionalization of carbon buckypaper for the sensitive determination of hydrogen peroxide in human urine, *Biosens. Bioelectron.*, 2012, **35**(1), 302–307.